Journal of Applied Physics ARTICLE pubs.aip.org/aip/jap

Huge mobility difference between the neutral and charged steps on 180° domain walls of $PbTiO_3$ by first-principles calculations

Cite as: J. Appl. Phys. **135**, 044104 (2024); doi: 10.1063/5.0176175
Submitted: 11 September 2023 · Accepted: 6 January 2024 ·
Published Online: 31 January 2024

Zhong Fang,[1,2] Yu-Jia Wang,[1,a)] Yun-Long Tang,[1] Yin-Lian Zhu,[3,4] and Xiu-Liang Ma[3,5]

AFFILIATIONS

[1]Shenyang National Laboratory for Materials Science, Institute of Metal Research, Chinese Academy of Sciences, Wenhua Road 72, Shenyang 110016, China
[2]School of Materials Science and Engineering, University of Science and Technology of China, Wenhua Road 72, Shenyang 110016, China
[3]Songshan Lake Materials Laboratory, Dongguan 523808, Guangdong, China
[4]School of Materials Science and Engineering, Hunan University of Science and Technology, Xiangtan 411201, China
[5]Institute of Physics, Chinese Academy of Sciences, Beijing 100190, China

[a)]**Author to whom correspondence should be addressed:** yjwang@imr.ac.cn

ABSTRACT

The microscopic mechanism of ferroelectric switching is the motion of domain walls, which is actually accomplished by the movement of tiny steps on the domain walls. Using first-principles calculations, the detailed polarization structures and the motion barriers of neutral and charged steps on 180° domain walls of prototypical ferroelectrics $PbTiO_3$ are elaborately revealed in this study. While the Bloch components get weakened near all neutral steps, they become weakened/strengthened near the head-to-head/tail-to-tail charged steps. The neutral step possesses a lower formation energy but a higher migration barrier, indicating that the charged step could move faster. Based on these results, the possible motion picture of steps on one 180° domain wall of tetragonal ferroelectrics is proposed, which provides a better understanding of the mechanism of domain wall motion and may shed light on the future development of domain wall–based functional devices.

I. INTRODUCTION

Ferroelectric materials have attracted tremendous research interest for decades because of their versatile physical properties. Ferroelectric domain walls (DWs) are ubiquitous in ferroelectric materials, which are found to possess unique internal structures[1–6] and physical properties, such as enhanced conductivity,[7–10] abnormal photovoltaic properties,[11,12] flexoelectricity,[13,14] electro-optical properties,[15–17] and so on. They have been considered as the basis for versatile applications including nonvolatile random-access memory, piezoelectric actuators, and pyroelectric detectors.[18,19] Therefore, it is of great scientific and technological significance to study DWs.

The properties of DWs are mainly governed by local polarization profiles. Ferroelectric 180° DWs generally exhibit predominantly Ising-like features, where the polarization vector only reverses its direction without rotation as it passes through the DWs.[20,21] In analogy to magnetic DWs, ferroelectric 180° DWs can also exhibit mixed characteristics with various collocations of the polarization components, such as Ising–Néel,[6,22] Ising–Bloch,[2,3] and Ising–Bloch–Néel.[1,4,13,23–26] For example, the prototype [1 0 0]- and [1 1 0]-oriented 180° DWs in $PbTiO_3$ (PTO) have been widely recognized as Ising–Bloch–Néel type,[4,26] as illustrated in Fig. 1(a).

In addition to the static property, the motion of DWs, which is the result of the repeated nucleation and growth of tiny steps (also termed "kinks" in the literature[27]) along existing parent DWs, has attracted great attention.[28–33] Meanwhile, achieving controlled motion of ferroelectric DWs is of great importance for the development of domain wall-based devices. Currently, the main control schemes include electric fields and strain fields.[34–38] In addition, polarized light has been reported to control the movement of BTO

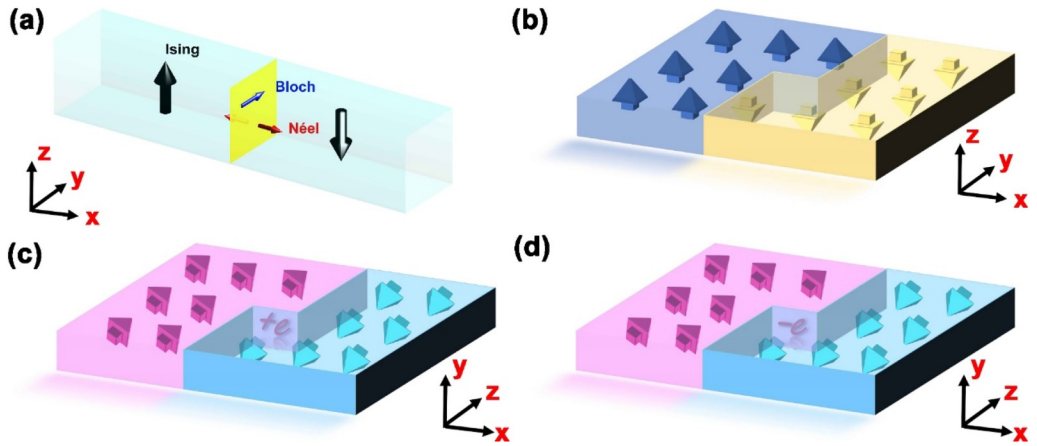

FIG. 1. The schematic diagrams of DW chirality and step structures. (a) A schematic diagram of the Ising, Néel, and Bloch type polarization components for a 180° DW model, where the yellow surface represents a typical 180° DW. (b) A neutral step model with polarization parallel to the step plane and no charge accumulation. (c) A tail-to-tail charged step model with negative bound charges. (d) A head-to-head charged step model with positive bound charges.

DWs.[39] The originally proposed Miller–Weinreich step motion model,[28] which did not address the fine structures of the steps, resulted in a severe underestimation of the DW motion velocity, because of the high potential barrier derived from the overestimation of the polarization gradient around the steps.[40] To overcome this drawback, Shin *et al.* proposed the diffusion-boundary model, which is in better agreement with the experiment because of the detailed analysis of the polarization distribution around the steps.[31] According to the distribution of polarization around the steps, the steps can be classified as neutral steps, tail-to-tail steps with negative bound charges, and head-to-head steps with positive bound charges, as shown in the schematic diagrams of Figs. 1(b)–1(d). Using the method of anharmonic lattice statics, Angoshtari and Yavari plotted the distribution of polarization near the neutral steps of PTO and compared the energy differences of neutral steps with various element compositions but did not address the charged steps.[41] Jiang *et al.* studied the distribution of polarization and bound charges in the vicinity of charged steps by first-principles calculations and further investigated the DW-orientation-modulated vortex structures but did not rigorously calculate the moving barriers of the steps.[42,43]

In this work, we have investigated neutral and charged steps in tetragonal PTO by means of first-principles calculations. We mainly focused on the polarization structures of charged and neutral steps and explored their motion barriers by the nudged elastic band method. The introduction of steps can effectively influence the Ising–Bloch–Néel polarization distribution of the 180° DWs of PTO. The charged step possesses a larger formation energy and migrates much faster. Our work can provide insight into the DW motion mechanism and the development of DW-based functional devices in the future.

II. THEORETICAL DETAILS

A. Model geometries

The fully relaxed structure of the bulk PTO tetragonal phase (P4 mm) was applied in all the following supercells. Considering the element composition and charge state of the step planes, there are totally four prototypes of step models, as depicted in Fig. 2. For all models, only Pb-centered DWs are considered, since Pb-centered 180° DWs have been demonstrated to be the most stable.[21] Apparently, there are two steps in each model attributed to the periodic boundary condition.

In order to determine the appropriate model size, a series of $M \times 1 \times N$ supercells ($M = 6$, 8, 10, 12, 14, and 16 and $N = 4$, 6, 8, and 10) have been calculated in this work, where M and N represent the number of cells in directions that are perpendicular and parallel to the DWs, respectively, and 1 represents a periodicity of 1 unit cell in the normal direction of the paper, as shown in Fig. 2. For the neutral step model, M and N represent the number of unit cells along the x and y axes, while for the charged step models, M and N represent the number of unit cells along the x and z axes, respectively. To save computation cost, only one unit cell was chosen in the direction normal to the paper. In other words, our models are two-dimensional. Brillouin-zone integrations were performed with $6 \times 6 \times 6$, $1 \times 6 \times 3$, $1 \times 6 \times 1$ Monkhorst–Pack[44] k-point meshes for the bulk, the $M \times 1 \times 2$ supercells, and the $M \times 1 \times N$ supercells ($N = 4$, 6, 8, and 10), respectively. To determine the appropriate horizontal dimension of the model, we calculated a series of models with sizes of $M \times 1 \times 4$, as shown in Fig. 2. We considered the horizontal dimension of the model to be beyond the influence of the DWs when the polarization of the unit cell away from the DWs converged to the bulk value. Striking a balance between computational effort and accuracy, the horizontal dimension was chosen as $M = 8$. To determine the dimension of the step models along the vertical direction (the value of N), a series of models with sizes of $8 \times 1 \times N$ were constructed and the Ising polarization profiles across the DW were fitted by using the Landau–Ginzburg–Devonshire (LGD) theory.[20,21] The Ising polarization component P_z could be fitted to the one-dimensional

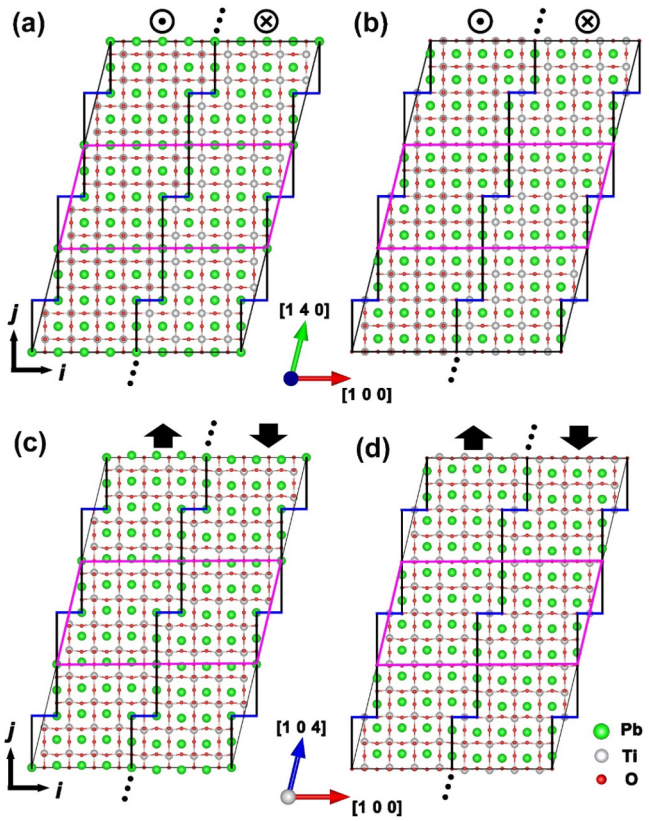

FIG. 2. Atomic models of four types of steps. (a) and (b) are neutral step models with polarization parallel to the step planes of PbO and TiO_2, respectively. (c) and (d) are charged step models with step planes of PbO and TiO_2, respectively. The polarization directions of the domains are marked by the black orientation symbols, and the black and blue solid lines represent the DWs and step planes, respectively. The pink boxes represent periodic supercells. To reveal the step models more clearly, three periods are shown in the direction parallel to the domain walls.

solution of the 180° DW from the sixth-order LGD theory,

$$P_z(x) = P_z^0 \frac{\sinh\left(\frac{x - x_0}{\xi}\right)}{\left[1 + \sinh^2\left(\frac{x - x_0}{\xi}\right)\right]^{\frac{1}{2}}}, \quad (1)$$

where P_z^0 is the magnitude of the polarization in the bulk, ξ denotes the half width of the DW, and x_0 represents the position where the fitting curve crosses the zero line and is considered as the specific position of the DW center. This fitting method has successfully described the relationship between polarization distribution and the position of ferroelectric DWs in many works.[1,22,42] The fitting results suggest that $8 \times 1 \times 10$ supercells would be the appropriate scale for both neutral and charged steps. All subsequent models will be set to this scale, and the lattice parameters of these supercells are not changed during the relaxation process. It is well known that there exists large Bloch-type components at the 180° DWs of PTO.[3,4,26] In the initial models, the Bloch-type components were introduced in the 180° DWs.

B. Calculation details

In the present study, all simulations are performed with density functional theory (DFT) using the projector augmented wave (PAW) method[45] as incorporated in the Vienna *ab initio* simulation package (VASP).[46,47] The valence electrons of Pb, Ti, and O are chosen as $5d^{10}6s^26p^2$, $3s^23p^63d^24s^2$, and $2s^22p^4$, respectively.[13] An energy cutoff of 500 eV was used for all computations. The convergence conditions for the electronic self-consistent loop were set at 10^{-5} eV, while the ionic relaxation loop was considered convergent when the forces on all atoms were less than 0.01 eV $Å^{-1}$. It should be noted that a Hubbard U correction is often adopted for the treatment of 3d electrons of Ti, which can describe the electronic structure more accurately.[48] We performed the LDA + U calculations for the bulk PTO and the results are listed in Table I. As shown in this table, polarization and tetragonality decrease with the increase in the U value. The lattice parameters and the spontaneous polarization at the LDA level are close to the experimental values[49–51] and previous calculations.[42] Thus, the LDA is chosen in our following calculations.

For a precise description of the polarization distribution, we induced superscript indices i and j to label every unit cell in the models along the horizontal and vertical directions, respectively. The polarization of the unit cell ij was calculated by means of the following formula:[52]

$$P^{ij} = \frac{e}{\Omega_c} \sum w_\alpha Z_\alpha^* u_\alpha^{ij}, \quad (2)$$

where e is the electron charge, Ω_c is the volume of one unit cell, w_α is the weight factor of the α ion (Pb, Ti, or O) in the unit cell, Z_α^* is the Born effective charge of the α ion, and u_α^{ij} is the offset of the α ion in the unit cell ij relative to its cubic position. The calculated

TABLE I. A comparison of structural parameters and polarization calculated by the LDA + U method for the bulk PTO with experiments and other theoretical calculations, where U ranges from 0 to 6 eV. The units of lattice parameter a and the spontaneous polarization P are Å and $\mu C/cm^2$, respectively.

LDA + U									
U	0	1	2	3	4	5	6	Exp.[49–51]	Theory[42]
a	3.866	3.882	3.894	3.906	3.915	3.923	3.931	3.899	3.867
c/a	1.043	1.030	1.020	1.013	1.008	1.006	1.004	1.065	1.043
P	78.38	69.56	61.36	53.99	47.33	42.77	39.83	75.00	83.00

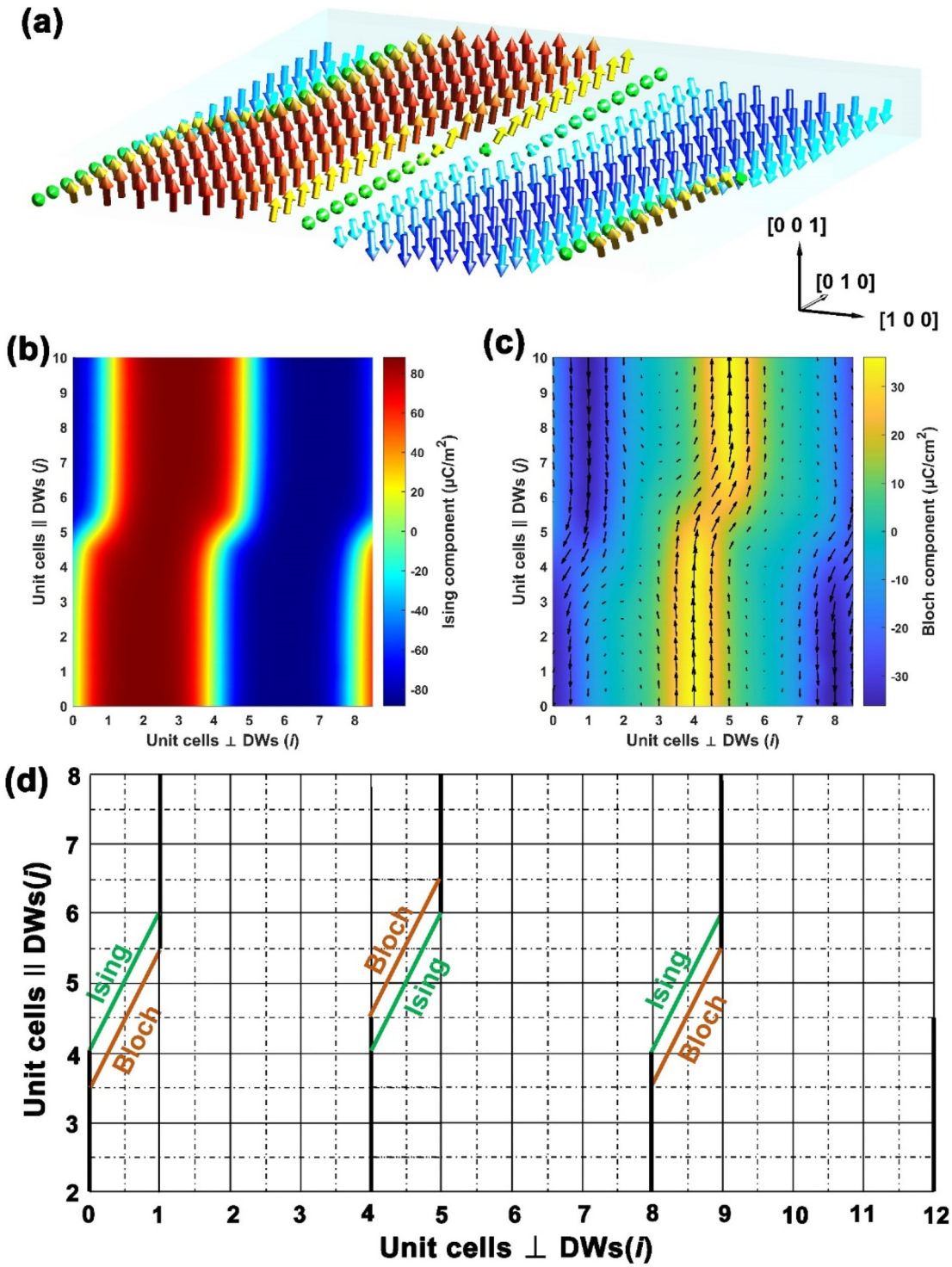

FIG. 3. Various polarization component distributions of a neutral step. (a) The three-dimensional polarization vector distribution of the model. (b) and (c) correspond to the distributions of Ising and Bloch components, respectively. (d) shows the step planes fitted by Ising and Bloch components. To reveal the schematic step planes more clearly, a 1.5 period is shown in the direction perpendicular to the domain walls.

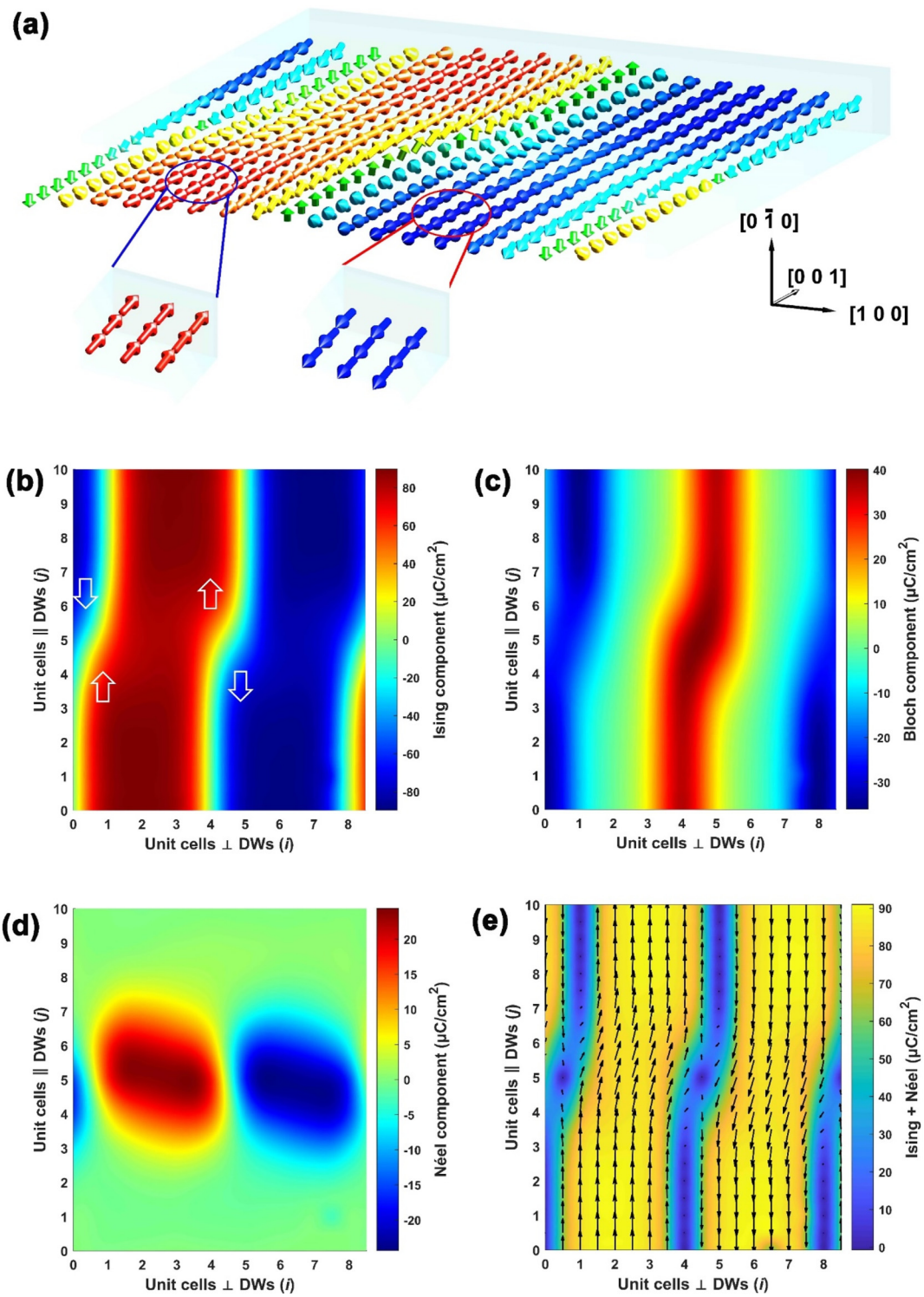

FIG. 4. Different polarization component distributions of a charged step. (a) A three-dimensional polarization vector distribution. (b)–(d) correspond to the Ising, Bloch, and Néel component distributions, respectively. (e) A projection of the polarization vectors onto the (0 1 0) plane.

TABLE II. Calculated formation energies and potential barriers of different steps.

Energy	Neutral step	Charged step
Formation energy (10^{-11} J/m)	1.37	3.00
Potential barrier (10^{-11} J/m)	0.77	0.07

Born effective charges for all atoms are extracted from the cubic PTO.

III. RESULTS AND DISCUSSIONS

A. The structures of neutral steps

After full relaxation, the three-dimensional polarization vector distribution of the model with the step plane of the PbO (0 1 0) crystallographic plane [Fig. 2(a)] is shown in Fig. 3(a), where polarizations at the domain centers are uniform and converge to the bulk value, indicating that the adjacent steps and DWs are well separated. The mapping of Ising polarization components is plotted in Fig. 3(b). The projection of the Ising component reveals that the step planes deviate greatly from the initially set PbO (0 1 0) crystallographic plane. The new inclined step extends about two unit cells along the vertical direction, which corresponds to the PbO (2 $\bar{1}$ 0) one. In addition, it is worth noting that if the step plane is set to be the TiO_2 (0 1 0) plane, as depicted in Fig. 2(b), the relaxed structure is still the PbO (2 $\bar{1}$ 0) plane instead of the expected TiO_2 (2 $\bar{1}$ 0) plane. The unexpected disappearance of the TiO_2 (2 $\bar{1}$ 0) plane will be reasonably explained in the discussion on potential barriers later. The distribution of the Bloch component after full relaxation is depicted in Fig. 3(c), with the in-plane polarization vectors. The in-plane polarization vectors are always parallel to the DWs, for both the regions of the pristine DWs and the step planes. Beside this feature, the striking difference between Figs. 3(b) and 3(c) is that the step position determined by the Bloch polarization distribution (step B) is different from that obtained by the Ising one (step I), which is schematically shown in Fig. 3(d). It should be emphasized that the plot in Fig. 3(d) is based on periodic boundary conditions. Combining Figs. 3(c) and 3(d), it is found that for the DW with positive Bloch components ($i = 4$–5), step B is half unit cell above step I and for the DW with negative Bloch components ($i = 0$–1 or 8–9), step B is half unit cell below step I. In other words, step B is always a half unit cell away from step I in the direction of the Bloch components.

B. The structures of charged steps

The distribution of the polarization components of the charged step model with the step plane of the PbO (0 0 1) crystallographic plane [Fig. 2(c)] after full relaxation is shown in Fig. 4. Analogous to the neutral step, the three-dimensional polarization vector mapping is shown in Fig. 4(a). The distributions of different polarization components are, respectively, depicted in Figs. 4(b)–4(d). The crystallographic plane of the charged step is the PbTiO (3 0 $\bar{1}$) plane, since the step extends about three unit cells in the vertical direction, and the charged step model with the initial step plane of the TiO_2 (0 0 1) crystallographic plane [Fig. 2(d)] relaxed to the structure with the step plane of the O_2 (3 0 $\bar{1}$) plane (not shown here), which are both consistent with the previous study not considering the Bloch components.[42] As shown in Fig. 4(c), the distribution of the Bloch components in the vicinity of different steps shows opposite trends, with the Bloch components increasing near the tail-to-tail step and decreasing near the head-to-head one, which is different from the case of the neutral step. In the latter case, the Bloch components near both steps in one model decrease. The Néel component forms a centrosymmetric distribution around the steps because of the electrostatic potential difference between the head-to-head and tail-to-tail steps,[8,42] as shown in Fig. 4(d). The polarization vectors near the steps are tilted due to the bound charge of the charged step, forming the polar antivortex patterns [Fig. 4(e)], which is consistent with the previous literature.[43]

C. Step formation energies and motion barriers

The motion of the DWs can be considered as the nucleation and motion of the steps, which are related to the formation energy and the motion barriers of the steps from an energetic point of view, respectively. The step formation energy could be regarded as the energy difference between the step model and the corresponding ideal 180° DWs with the same size. Therefore, we adopt the following formula:

$$E_{\text{step}} = \frac{E_{\text{tot}} - E_{\text{dw}}}{2L}, \tag{3}$$

where E_{tot} is the energy of the step models with a size of $8 \times 1 \times 10$, E_{dw} is the energy of an $8 \times 1 \times 10$ supercell with pristine 180° DWs, and L is the unit length of the step ($L = c$ and a for the neutral and the charged steps). As shown in Table II, although the formation energy of a pair of neutral steps is lower than that of a pair of charged steps, the different is not so large, which indicates that both steps could nucleate on the 180° DWs.

We further calculated the step motion barriers by the nudged elastic band (NEB) approach. As shown in Figs. 5(a) and 5(b), the neutral and charged steps move from the initial equilibrium states (marked by ①) to the nearest-neighbor equilibrium states (marked by ②) as a motion cycle. Note that the distortion near the DWs in Fig. 5(b) is due to the converse flexoelectric effect.[14,50,53] The energy profiles along the migration paths of the neutral and charged steps are shown in Figs. 5(c) and 5(d), and the calculated potential barriers are shown in Table II. The structures corresponding to the saddle points of the above energy profiles happen to be the TiO_2 (2 $\bar{1}$ 0) and O_2 (3 0 $\bar{1}$) step planes, respectively. In Sec. III A, we have mentioned that the neutral step model with the TiO_2 (0 1 0) plane relaxed to the PbO (2 $\bar{1}$ 0) plane instead of the expected TiO_2 (2 $\bar{1}$ 0) plane. From Fig. 5(c), it is found that the energy profile is very steep near the saddle point. This is the reason why the step model with the TiO_2 (2 $\bar{1}$ 0) planes disappears during the atomic relaxation. In contrast, the energy profile is very flat near the saddle point for the charged step model, as shown in Fig. 5(d). As a result, the step model with the O_2(3 0 $\bar{1}$) step planes survives during the relaxation.

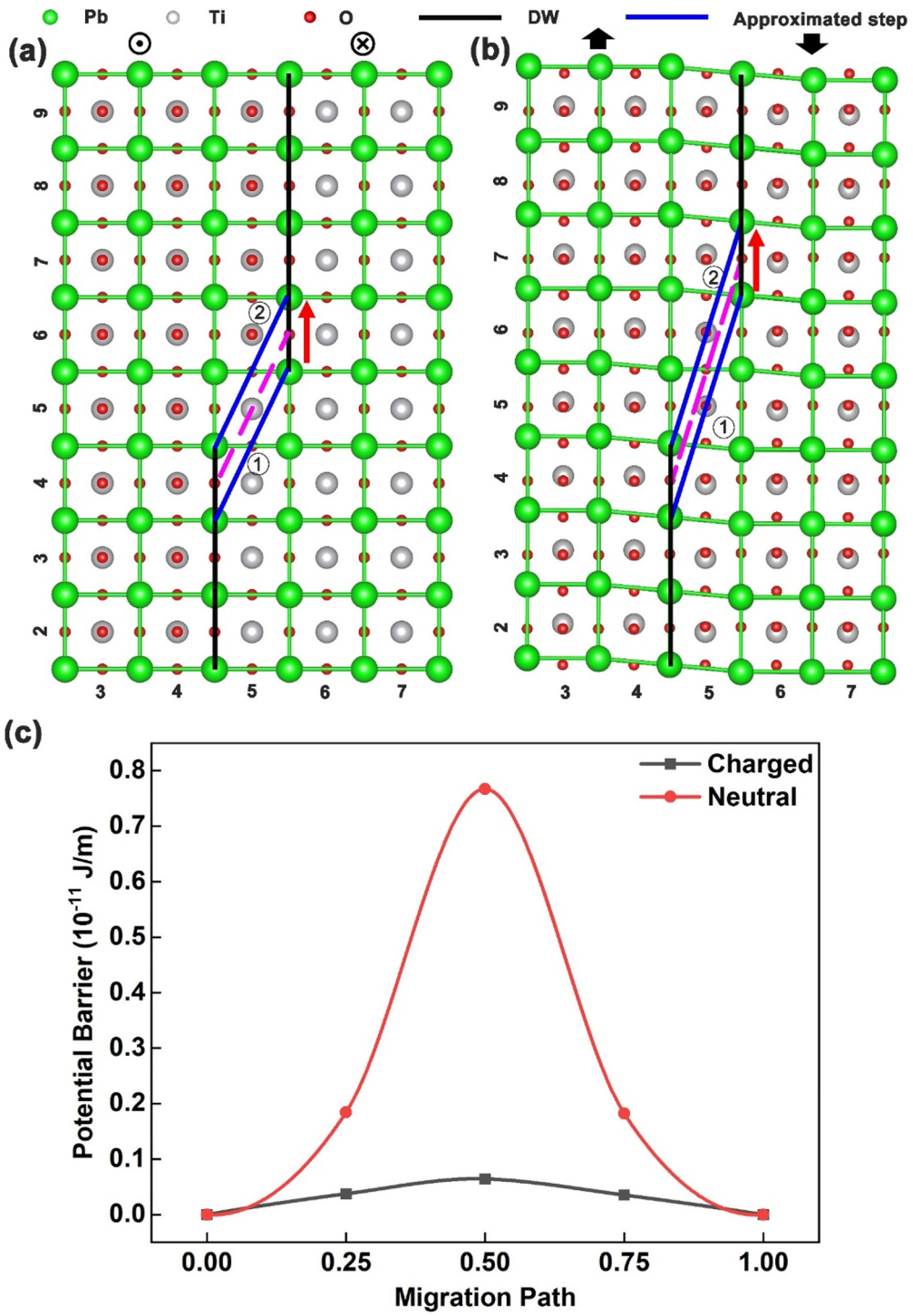

FIG. 5. (a) and (b) are the schematic diagrams of the motion process of the neutral and charged steps obtained by the NEB methods, respectively. The black solid lines represent the PbO DWs and blue solid lines represent the approximate crystallographic planes of the reassigned steps. The marks of ① and ② are the initial and final states, respectively. The pink dashed lines represent the saddle points. The red arrows indicate the motion directions of the steps. (c) represents the energy profiles along the migration path corresponding to charged and neutral steps, respectively.

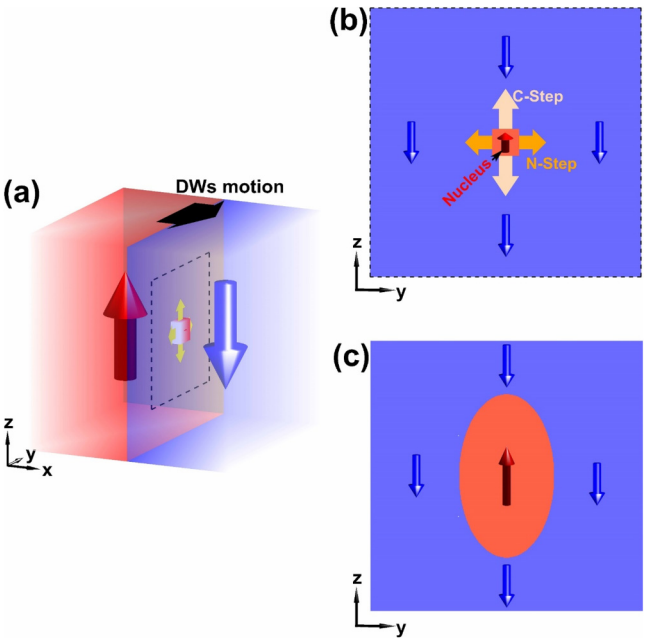

FIG. 6. (a) A schematic diagram of the 180° DW motion, where the steps extend along the DW, and the DW migrates rightward. (b) The steps and their growth directions in the vicinity of the nucleus. The length of the arrows qualitatively represents the growth rate. C-Step and N-step denote the charged step and the neutral step, respectively. (c) A schematic diagram of the nucleus growing along different directions on the DWs.

IV. DISCUSSION

The migration velocity of DWs can impact device performance. A faster migration velocity leads to a superior device performance, such as fast reading and writing of the storage device. Investigating the differences in the motion speed of the different steps will undoubtedly be instructive for device development. For decades, Merz's law has been widely and successfully used as a well-known empirical formula to describe the relationship between the DW motion speed and the applied electric field: $v \propto \exp(-E_a/E)$, where E_a is the applied electric field and E_a is the activation field usually obtained by data fitting without a clear physical definition.[28,40,54,55] Due to the huge difference in the potential barriers of different steps, it is reasonable to infer that the activation field of the charged step is much smaller than that of the neutral one. According to Merz's law, the migration speed of the neutral step should be much lower than that of the charged step. Here, we plot a schematic diagram of the 180° DW motion mechanism, as shown in Fig. 6, in which the DW migrates rightward, and the tiny step nucleates and expands on the DW. According to the polarization distribution in the proximity of the nucleus, there will be neutral and charged steps, and their motion directions on the DW are shown in Fig. 6(b). Due to the difference in the motion velocity of the steps, the nucleus expands much faster in the z-direction than in the y-direction, as depicted in Fig. 6(c). In other words, the growth velocity of the nucleus in the y-direction dominates the migration speed of the DWs.

V. CONCLUSION

In summary, we have systematically carried out a comparative study of neutral and charged steps on 180° domain walls in a classical ferroelectric, $PbTiO_3$, using first-principles calculations, focusing on the polarization structures and the motion barriers. The main conclusions are listed below:

(1) The neutral step plane determined by the Bloch components is always a half unit cell away from that by the Ising ones in the direction of the Bloch components, whereas the Bloch components get weakened near the head-to-head step and strengthened near the tail-to-tail step.
(2) The formation energies of the neutral and charged steps are comparative, indicating that both steps could form on 180° domain walls.
(3) The motion barrier of the charged steps is much smaller than that of the neutral ones, which indicates that the charged steps could migrate much faster than the neutral ones.

ACKNOWLEDGMENTS

The authors thank Dr. Y. X. Jiang of the Institute of Metal Research, Chinese Academy of Sciences, for the discussion about the model construction. This work was supported by the National Natural Science Foundation of China (Nos. 52122101 and 51971223) and the Shenyang National Laboratory for Materials Science (Nos. L2019R06, L2019R08, L2019F01, L2019F13). Y.-J.W. and Y.-L.T. acknowledge the Youth Innovation Promotion Association CAS (Nos. 2021187 and Y202048). Y.-L.T. acknowledges the Scientific Instrument Developing Project of CAS (No. YJKYYQ20200066).

AUTHOR DECLARATIONS

Conflict of Interest

The authors declare that they have no known competing financial interests or personal relationships that could have appeared to influence the work reported in this paper.

Author Contributions

Zhong Fang: Data curation (lead); Visualization (lead); Writing – original draft (lead). **Yu-Jia Wang:** Conceptualization (lead); Funding acquisition (equal); Supervision (lead); Writing – review & editing (lead). **Yun-Long Tang:** Funding acquisition (equal). **Yin-Lian Zhu:** Funding acquisition (equal). **Xiu-Liang Ma:** Funding acquisition (equal).

DATA AVAILABILITY

The data that support the findings of this study are available from the corresponding author upon reasonable request.

REFERENCES

[1]D. Lee, R. K. Behera, P. Wu, H. Xu, Y. L. Li, S. B. Sinnott, S. R. Phillpot, L. Q. Chen, and V. Gopalan, Phys. Rev. B **80**, 060102 (2009).
[2]M. Taherinejad, D. Vanderbilt, P. Marton, V. Stepkova, and J. Hlinka, Phys. Rev. B **86**, 155138 (2012).
[3]J. C. Wojdeł and J. Íñiguez, Phys. Rev. Lett. **112**, 247603 (2014).
[4]Y. J. Wang, D. Chen, Y. L. Tang, Y. L. Zhu, and X. L. Ma, J. Appl. Phys. **116**, 224105 (2014).
[5]C. L. Jia, L. Jin, D. W. Wang, S. B. Mi, M. Alexe, D. Hesse, H. Reichlova, X. Marti, L. Bellaiche, and K. W. Urban, Acta Mater. **82**, 356 (2015).
[6]G. De Luca, M. D. Rossell, J. Schaab, N. Viart, M. Fiebig, and M. Trassin, Adv. Mater. **29**, 1605145 (2017).
[7]J. Seidel, L. W. Martin, Q. He, Q. Zhan, Y. H. Chu, A. Rother, M. E. Hawkridge, P. Maksymovych, P. Yu, M. Gajek, N. Balke, S. V. Kalinin, S. Gemming, F. Wang, G. Catalan, J. F. Scott, N. A. Spaldin, J. Orenstein, and R. Ramesh, Nat. Mater. **8**, 229 (2009).
[8]E. A. Eliseev, A. N. Morozovska, G. S. Svechnikov, P. Maksymovych, and S. V. Kalinin, Phys. Rev. B **85**, 045312 (2012).
[9]P. Bednyakov, T. Sluka, A. Tagantsev, D. Damjanovic, and N. Setter, Adv. Mater. **28**, 9498 (2016).
[10]M. P. Campbell, J. P. V. McConville, R. G. P. McQuaid, D. Prabhakaran, A. Kumar, and J. M. Gregg, Nat. Commun. **7**, 13764 (2016).
[11]S. Y. Yang, J. Seidel, S. J. Byrnes, P. Shafer, C. H. Yang, M. D. Rossell, P. Yu, Y. H. Chu, J. F. Scott, J. W. Ager 3rd, L. W. Martin, and R. Ramesh, Nat. Nanotechnol. **5**, 143 (2010).
[12]A. Bhatnagar, A. Roy Chaudhuri, Y. Heon Kim, D. Hesse, and M. Alexe, Nat. Commun. **4**, 2835 (2013).
[13]Y. J. Wang, J. Y. Li, Y. L. Zhu, and X. L. Ma, J. Appl. Phys. **122**, 224101 (2017).
[14]Y. J. Wang, Y. L. Tang, Y. L. Zhu, Y. P. Feng, and X. L. Ma, Acta Mater. **191**, 158 (2020).
[15]A. A. Demkov, J. E. Ortmann, M. Reynaud, A. K. Hamze, P. Ponath, and W. T. Li, Phys. Status Solidi B **258**, 2000497 (2021).
[16]M. Reynaud, Z. M. Dong, H. Park, W. T. Li, A. B. Posadas, J. H. Warner, D. Wasserman, and A. A. Demkov, Phys. Rev. Mater. **6**, 095201 (2022).
[17]W. T. Li, C. M. Landis, and A. A. Demkov, Phys. Rev. Mater. **6**, 095203 (2022).
[18]G. Catalan, J. Seidel, R. Ramesh, and J. F. Scott, Rev. Mod. Phys. **84**, 119 (2012).
[19]D. Meier and S. M. Selbach, Nat. Rev. Mater. **7**, 157 (2022).
[20]W. Cao, G. R. Barsch, and J. A. Krumhansl, Phys. Rev. B **42**, 6396 (1990).
[21]W. Cao and L. E. Cross, Phys. Rev. B **44**, 5 (1991).
[22]R. K. Behera, C. W. Lee, D. Lee, A. N. Morozovska, S. B. Sinnott, A. Asthagiri, V. Gopalan, and S. R. Phillpot, J. Phys.: Condens. Matter **23**, 175902 (2011).
[23]Y. Gu, M. Li, A. N. Morozovska, Y. Wang, E. A. Eliseev, V. Gopalan, and L. Q. Chen, Phys. Rev. B **89**, 174111 (2014).
[24]M. Li, Y. Gu, Y. Wang, L. Q. Chen, and W. Duan, Phys. Rev. B **90**, 054106 (2014).
[25]Y. J. Wang, Y. L. Zhu, and X. L. Ma, J. Appl. Phys. **122**, 134104 (2017).
[26]X. Y. Zhang, B. Wang, Y. Z. Ji, F. Xue, Y. Wang, L. Q. Chen, and C. W. Nan, Acta Mater. **242**, 118351 (2023).
[27]J. Gonnissen, D. Batuk, G. F. Nataf, L. Jones, A. M. Abakumov, S. Van Aert, D. Schryvers, and E. K. H. Salje, Adv. Funct. Mater. **26**, 7599 (2016).
[28]R. C. Miller and G. Weinreich, Phys. Rev. B **117**, 1460 (1960).
[29]R. E. Nettleton, J. Phys. Soc. Jpn. **22**, 1375 (1967).
[30]A. Grigoriev, D. H. Do, D. M. Kim, C. B. Eom, B. Adams, E. M. Dufresne, and P. G. Evans, Phys. Rev. Lett. **96**, 187601 (2006).
[31]Y. H. Shin, I. Grinberg, I. W. Chen, and A. M. Rappe, Nature **449**, 881 (2007).
[32]S. Liu, I. Grinberg, and A. M. Rappe, Nature **534**, 360 (2016).
[33]X. Y. Li, Q. Yang, J. X. Cao, L. Z. Sun, Q. X. Peng, Y. C. Zhou, and R. X. Zhang, J. Phys. Chem. C **122**, 3091 (2018).
[34]E. J. Guo, R. Roth, A. Herklotz, D. Hesse, and K. Dörr, Adv. Mater. **27**, 1615 (2015).
[35]L. J. McGilly, P. Yudin, L. Feigl, A. K. Tagantsev, and N. Setter, Nat. Nanotechnol. **10**, 145 (2015).
[36]R. J. Xu, S. Liu, I. Grinberg, J. Karthik, A. R. Damodaran, A. M. Rappe, and L. W. Martin, Nat. Mater. **14**, 79 (2015).
[37]S. R. Bakaul, J. Kim, S. Hong, M. J. Cherukara, T. Zhou, L. Stan, C. R. Serrao, S. Salahuddin, A. K. Petford-Long, D. D. Fong, and M. V. Holt, Adv. Mater. **32**, 1907036 (2020).
[38]Z. Liu, H. Wang, M. Li, L. Tao, T. R. Paudel, H. Yu, Y. Wang, S. Hong, M. Zhang, Z. Ren, Y. Xie, E. Y. Tsymbal, J. Chen, Z. Zhang, and H. Tian, Nature **613**, 656 (2023).
[39]F. Rubio-Marcos, A. Del Campo, P. Marchet, and J. F. Fernández, Nat. Commun. **6**, 6594 (2015).
[40]T. Tybell, P. Paruch, T. Giamarchi, and J. M. Triscone, Phys. Rev. Lett. **89**, 097601 (2002).
[41]A. Angoshtari and A. Yavari, J. Appl. Phys. **108**, 084112 (2010).
[42]Y. X. Jiang, Y. J. Wang, D. Chen, Y. L. Zhu, and X. L. Ma, J. Appl. Phys. **122**, 054101 (2017).
[43]Y. X. Jiang, Y. J. Wang, D. Chen, Y. L. Zhu, and X. L. Ma, Philos. Mag. Lett. **98**, 266 (2018).
[44]H. J. Monkhorst and J. D. Pack, Phys. Rev. B **13**, 5188 (1976).
[45]P. E. Blöchl, Phys. Rev. B **50**, 17953 (1994).
[46]G. Kresse and J. Furthmüller, Comput. Mater. Sci. **6**, 15 (1996).
[47]J. Hafner, Comput. Phys. Commun. **177**, 6 (2007).
[48]W. T. Li, L. Y. Gao, and A. A. Demkov, Phys. Rev. B **102**, 035308 (2020).
[49]A. M. Glazer and S. A. Mabud, Acta Crystallogr., Sect. B **34**, 1065 (1978).
[50]Y. L. Tang, Y. L. Zhu, X. L. Ma, A. Y. Borisevich, A. N. Morozovska, E. A. Eliseev, W. Y. Wang, Y. J. Wang, Y. B. Xu, Z. D. Zhang, and S. J. Pennycook, Science **348**, 547 (2015).
[51]Y. J. Wang, Y. P. Feng, Y. L. Zhu, Y. L. Tang, L. X. Yang, M. J. Zou, W. R. Geng, M. J. Han, X. W. Guo, B. Wu, and X. L. Ma, Nat. Mater. **19**, 881 (2020).
[52]B. Meyer and D. Vanderbilt, Phys. Rev. B **65**, 104111 (2002).
[53]Y. L. Tang, Y. L. Zhu, Z. J. Hong, E. A. Eliseev, A. N. Morozovska, Y. J. Wang, Y. Liu, Y. B. Xu, B. Wu, L. Q. Chen, S. J. Pennycook, and X. L. Ma, J. Mater. Res. **32**, 957 (2017).
[54]W. J. Merz, Phys. Rev. **95**, 690 (1954).
[55]R. C. Miller and A. Savage, Phys. Rev. B **115**, 1176 (1959).